Hydrothermal Route Synthesis & Characterization of MoO_2/rGO Nanocomposites for Supercapacitor Applications

V. Ramanjaneyulu[1], K. Peddintaiah[1], Ch. Maneesha[1], A. Rajasekhar Babu[1]

[1] *Department of Chemical Engineering, JNTUA College of Engineering, Ananthapuramu, India*

* *Corresponding author Name: V. Ramanjaneyulu, email: ramanjaneyulu.chem@jntua.ac.in*

Abstract:

In this study, Cerium oxide and Cerium oxide/reduced grapheme oxide nanocomposites (MoO_2 and MoO_2/rGO NCs) were synthesized via a hydrothermal route and characterized using Powder X-ray Diffraction (XRD), Transmission Electron Microscopy (TEM), Scanning Electron Microscope (SEM), and Diffuse Reflectance Spectroscopy (DRS) techniques. PXRD confirmed a face-centered cubic (Fm-3m) structure with high crystallinity. TEM analysis showed a (040) lattice fringe width of 0.648 nm, closely matching the theoretical value (0.65nm). Optical bandgap were 2.75 eV (CeO_2) and 2.62 eV (CeO_2/rGO NCs). Electrochemical measurements revealed specific capacitances of 159.1 Fg^{-1} (MoO_2) and 245.1 Fg^{-1} (MoO_2/rGO NCs) at 1 Ag^{-1}, with capacitance retention of 90-95% after 2000 cycles. MoO_2/rGO NCs also exhibited effective sensing performance for lead ions, indicating its potential for multifunctional electrochemical applications. The key result of this work is the multifunctional use of the as-synthesised materials, which shows their efficacy for sensors and efficient energy storage, opening the door for sustainable and multipurpose devices.

Keywords: MoO_2; MoO_2/rGO; Electrochemical studies; Sensors; Hydrothermal.

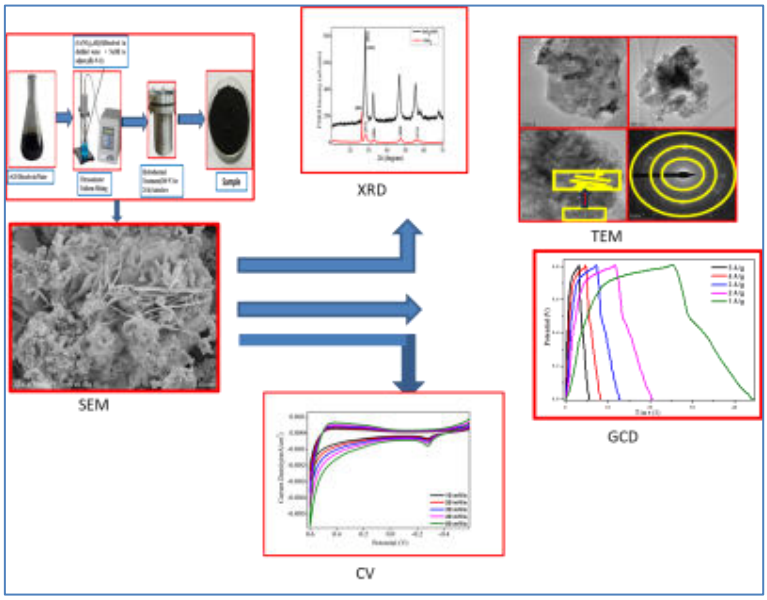

Fig.1. Graphical abstract of hydrothermally synthesized of MoO_2/rGO Nano Composites

1. Introduction:

An oxide of the rare-earth metal cerium, cerium (IV) oxide is often referred to as ceria or MoO_2. The powder is a light yellow-white colour. Both the melting and boiling points of MoO_2 are high (2,400°C and 3,500°C, respectively). It has a cubic crystal structure called the fluorite structure and is insoluble in water. Catalysis, fuel cells, oxygen sensors, and polishing agents all make extensive use of MoO_2 because of its superior physical and chemical characteristics [1-3]. MoO_2 is useful in applications requiring the storage and transport of oxygen because it has the ability to both release and absorb oxygen [4]. Cerium is a rare earth element that is most prevalent in the earth's crust, with an average concentration of 50 parts per million. It is a member of the lanthanide series. The shiny metal cerium is pliable and pliable. Cerium metal is extremely reactive and has an iron-gray hue. It's available as cerium oxide in conjunction with oxygen atoms and is also referred to as a potent oxidising agent [5]. This study focuses on molybdenum oxide (MoO_2), a prominent transition metal oxide known for its role as an n-type semiconductor. The material is characterized by a band gap ranging from 3 to 3.6 eV. These attributes render cerium oxide an ideal candidate for various applications, particularly in its nanoparticle form [7]. Because of their many uses in adsorption, fuel cells, hydrogen production, photocatalysis, catalysis, sensing, semiconductor devices, and the biomedical industry, cerium oxide-based nanomaterials have drawn a lot of interest [8].

MoO_2 has gained significant attention for its redox activity, oxygen storage capacity, and electrochemical behavior, making it a promising candidate for energy storage and sensing applications. However, its relatively low electrical conductivity limits its practical electrochemical performance. To overcome this limitation, reduced graphene oxide (rGO) is incorporated as a conductive support due to its high surface area, excellent electrical conductivity, and chemical stability. The MoO_2/rGO NCs synergistically combines the redox properties of MoO_2 with the conductive network of rGO, enhancing charge transport and electrochemical response. Recent studies have demonstrated similar enhancements using rGO-based composites, such as CuO@NiO/rGO for energy and environmental applications [9,10], and CuO@NiO/g-C_3N_4 for photocatalytic and electrochemical behavior [11].

Despite these advances, limited studies have addressed the dual application of MoO_2/rGONCs in both supercapacitor performance and heavy metal ion sensing. This work aims to fill that gap by synthesizing MoO_2 and MoO_2/rGO NCs via a facile hydrothermal

method and systematically investigating their structural, optical, and electrochemical properties. The novelty of the present study lies in the multifunctional deployment of the synthesized nanocomposites, demonstrating their superior performance with optimized morphology and interfacial interaction in energy storage and their electrochemical sensing capability for Pb^{2+} ions offering a cost-effective, sustainable platform for next-generation electrochemical devices.

In current study, the MoO_2 and MoO_2/rGO NCs were synthesized via a hydrothermal route using water as the solvent and avoiding any hazardous or toxic reagents. This method is considered environmentally friendly due to its energy efficiency, minimal waste generation, and non-toxic reaction conditions. The XRD spectra shows that the MoO_2 and MoO_2/rGO NCs a face-centered cubic (Fm-3m) structure with high crystallinity. High-Resolution Transmission Electron Microscopy (HR-TEM) analysis determined the fringe width value for the (040) plane to be 0.648 nm, which closely matches the theoretical value of 0.65 nm of the Mo NCs. The SEM images show irregular form and a structure like a flower with the nanocomposite clumped together.. Low charge resistance and high capacitance are correlated with a semicircle in the high-frequency area of MoO_2 and MoO_2/rGO NCs graphite electrode's impedance spectra, which also extends the electrode's sensor activity to lead. The key result of this work is the multifunctional use of the as-synthesised materials, which shows their efficacy for sensors and efficient energy storage, opening the door for sustainable and multipurpose devices.

2. Experimental:

2.1. Materials and Methods:

All chemicals were bought from (Sigma-Aldrich) Chemical house, Peenya Industrial area Bangalore-58, analytical grade used without purification. H_2O_2, Mo powder, ethylene glycol (>98%), including reduced graphene oxide (>99%). The procurement costs were reasonable and consistent with typical laboratory expenditures, ensuring accessibility and reproducibility for future studies.

2.2. Instruments:

A Shimadzu Powder X-ray Diffractometer (PXRD) equipped with a nickel filter was used to analyze the synthesized MoO_2 and MoO_2/rGO NCs. The measurements were conducted within an angular range of 20° to 70° using Cu Kα (1.541 Å) radiation at a scan rate of 2°

min^{-1}. The surface morphology of the nanocomposites was investigated using Hitachi SU1510 Scanning Electron Microscopy (SEM) and get high-resolution photographs of the material's structure. A JEOL 200CX microscope was used for the TEM investigation. DRS were recorded using a PerkinElmer UV spectrometer, while UV absorption spectra were analyzed using a Shimadzu UV spectrophotometer model 2600.

CV and EIS were carried out using a CHI608E electrochemical workstation configured with a three-electrode system. In this setup, a platinum wire was used as the counter electrode, a nickel mesh as the working electrode, and an Ag/AgCl electrode as the reference. All measurements were performed in an alkaline electrolyte of 1 M KOH. For EIS analysis, the frequency range spanned from 1 Hz to 1 MHz with applied AC signal amplitude of 5 mV.

2.3 . Synthesis of MoO_2 nanoparticles:

MoO_2 NPs were prepared via hydrothermal method. 10 mL 25 % H_2O_2 was added onto 1 gram Mo metal powder by continually stirring until the clear orange sol was obtained. Then the sol was mixed with 20 mL ethylene glycol and 55 mL deionized water. Stirring the sol for about 30 min until it turned into clear and yellow mixture, which was directly transferred into a Teflon-lined autoclave and operated at 200 ^{0}C for 72 h. Finally, the samples were centrifuged and washed by ethanol and deionized water for three times. After drying at 60 ^{0}C in vacuum condition for 24 h, the black powders were obtained.

2.4 . Synthesis of MoO_2/rGO nanocomposite:

The MoO_2/rGO NCs was prepared by hydrothermal method. To achieve optimal precursor concentrations for maximizing yield, an initial optimization process was conducted. The optimization of MoO_2 and rGO precursor concentrations were carried out by varying their ratios based on chemical stoichiometry and literature reports. A trial-and-error experimental design was used to identify the optimal formulation that yields nanocomposites with high crystallinity, desired morphology, and excellent electrochemical performance. The selected ratio consistently demonstrated superior characteristics across multiple batches, confirming the reliability and reproducibility of the optimized synthesis. According to the findings, 30 mL of 1 M ethylene glycol was ultrasonically treated with 0.04 g of rGO for 60 minutes. Following this, 0.02 g of MoO_2 was introduced after continuous stirring for 30 minutes.

The prepared solution was transferred into a Teflon-lined stainless steel autoclave and hydrothermally treated at 200°C for 24 hours. The resulting dark precipitate was cooled before being centrifuged and repeatedly cleaned with ethanol and distilled water until the final product turned transparent. The sample was ultimately dried in an oven at 60 °C for 24 hours, the black powders were obtained. The MoO_2/rGO NCs preparation is schematically depicted in Fig. 2.

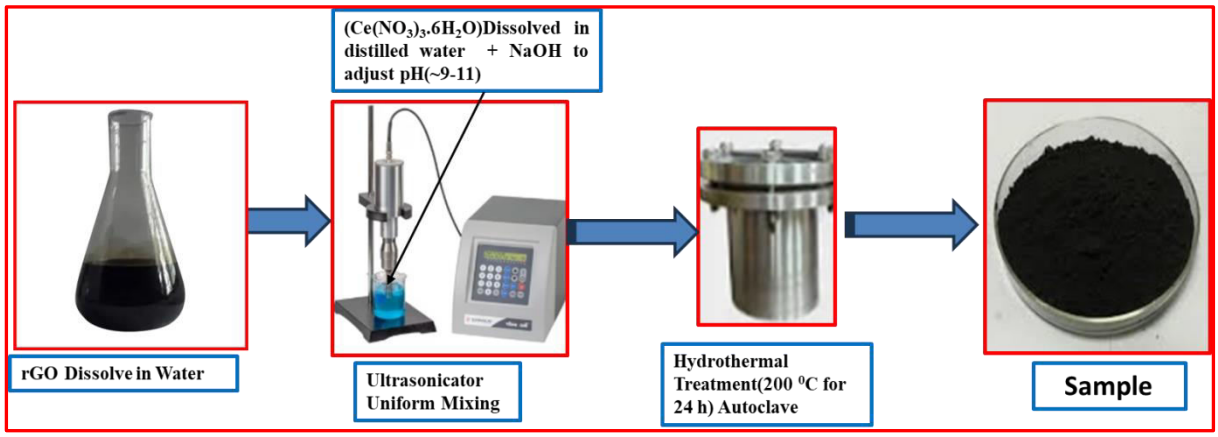

Fig.2. MoO_2 and MoO_2/rGO NCs synthesis is shown schematically.

2.5. Preparation of nickel mesh electrode of MoO_2/rGO NCs:

For electrode preparation, a total of 0.5 g of material was mixed in an agate mortar, consisting of 70 wt% MoO_2 or MoO_2/rGO NCs, 15 wt% graphite powder, and 15 wt% PTFE solution as a binder. The mixture was ground for approximately 45 minutes to form uniform slurry. This was then pressed onto a nickel mesh (Grade 200, mesh size: 100, thickness: ~0.2 mm, dimensions: 2 × 1 cm^2) using a hydraulic press at 20 MPa for 3 minutes to ensure strong electrical contact. The back side and wire connections were insulated with Teflon tape to define the active surface area and avoid short circuits during electrochemical measurements. Before use, the electrode was immersed in a 3 M KOH solution for about 30 minutes to ensure proper contact with the electrolyte [31,32].

2.6. Preparation of carbon paste electrode:

A carbon paste electrode with a 3 mm diameter was utilized as the working electrode for the CV analysis, while an Ag/AgCl electrode as reference electrode and platinum wire as counter electrodes, respectively. The experiment was conducted using a standard electrochemical cell setup. To ensure uniformity in the carbon paste electrode, graphite powder (70%) with a

density of 20 mg/100 mL and a mean particle size of 50 nm was thoroughly mixed with 15% silicone oil using a mechanical blending process. A weighing paper was then used to smooth the manufactured carbon paste after it had been inserted into a specially made carbon paste electrode. The analysis was performed using 1 M KOH as the electrolyte, at a scan rate of 10 mV/s [33,34].

3. Results and discussion:

3.1. Powder X-ray diffraction studies:

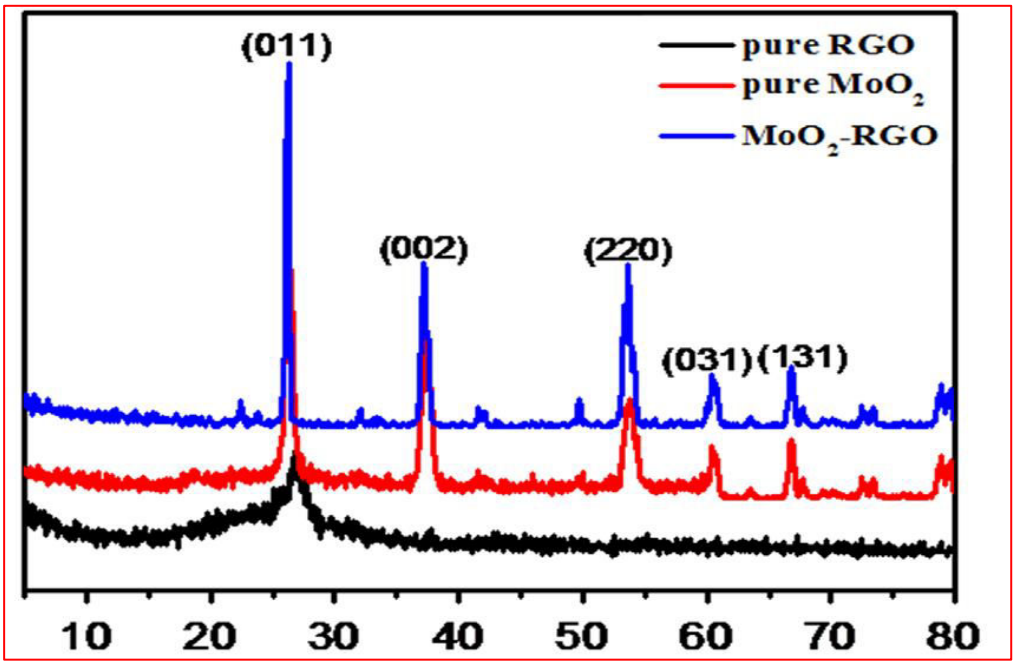

Fig.3. PXRD patterns of MoO_2 and MoO_2/rGO NCs.

The identified diffraction planes of MoO_2, (011) at ~26.26°, (002) at ~37.3°, (220) at ~53.8°, (031) at ~60.24°, (131) at ~66.7°, align well with JCPDS No. 65-5787. The synthesized MoO_2/rGO NCs possess a simple monoclinic structure with high crystallinity. The calculated lattice parameter for MoO_2/rGO NCs was found to be 0.5411 nm (a = b = c). The disappearance of the GO related peak at 10.4° and the appearance of a new peak at 27° typically suggest the formation of rGO[33-1]. However, it is important to note that rGO generally exhibits a broad (002) diffraction peak between 24–26° due to its disordered stacking and partial restoration of the graphitic structure.. The mean particle size of the nanocomposites was evaluated using the Debye Scherrer equation yielding an approximate size of 12.2 nm [36].

$$D = \frac{K\lambda}{\beta cos\theta} - - - - - (1)$$

Where θ represents the peak position (Bragg's angle), $\beta$is the full width at half maximum (FWHM), D denotes the mean crystallite size, K=0.9 is Scherrer constant, and λ is the X-ray wavelength. The corresponding SEM images further confirmed that the average crystallite size of MoO_2 and MoO_2/rGO NCs was approximately 12 nm.

3.2. Morphological studies:

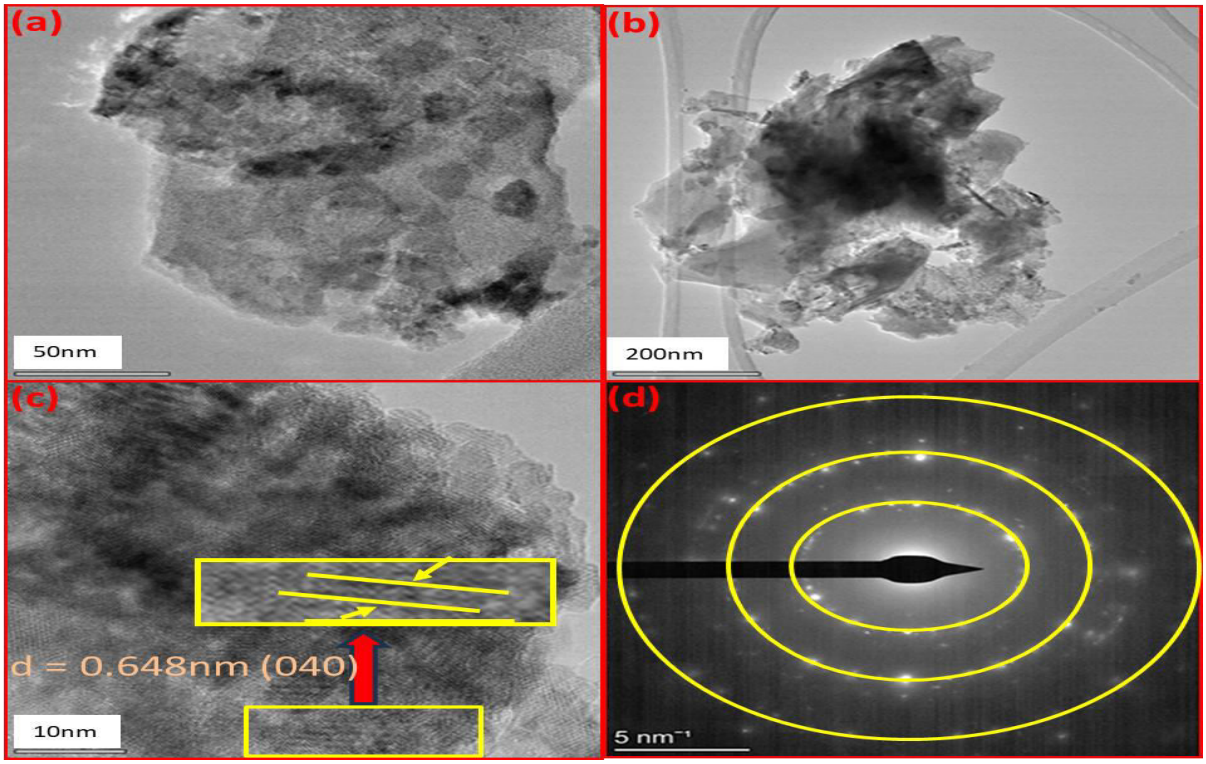

Fig. 4. (a & b) TEM images (c) HR TEM (d) SAED composition of MoO_2/rGO NCs.

The TEM images of the synthesized MoO_2/rGONCs are shown in Fig. 4(a & b). The size distribution of particles typically derived from measuring ~10nm particles. HR-TEM analysis determined the fringe width value for the (040) plane to be 0.648 nm, which closely matches the theoretical value of 0.65 nm, as illustrated in Fig. 4(c) [41]. The selected area electron diffraction (SAED) pattern, shown in Fig. 4(d), reveals. The materials crystalline nature through the presence of concentric rings corresponding to the crystal planes of (040), (021), (111), (002), and (112). The HR-TEM images clearly revealed well-dispersed MoO_2 nanoparticles anchored onto ultrathin, transparent, and wrinkled rGO nanosheets..

3.3 SEM analysis:

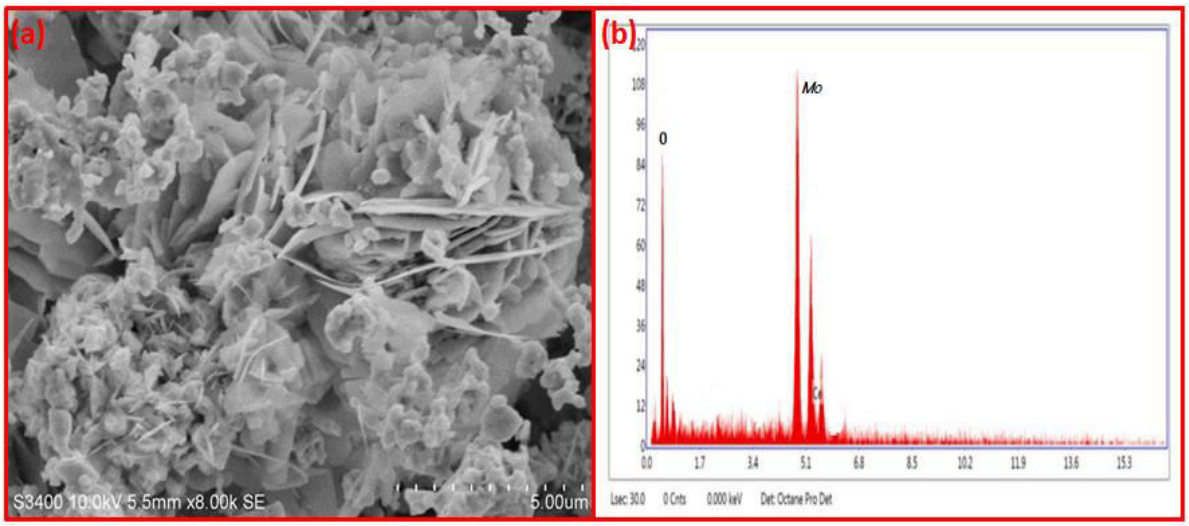

Fig. 5. (a) SEM **(b)** EDAX spectra of MoO_2/rGO NCs.

Fig.5a depict the morphological SEM image of the MoO_2/rGONCs, it reveals an irregular arrangement and flower like morphology with a nanocomposite clumped together with rGO. The energy dispersive X-ray (EDAX) analysis, presented in Fig.5b, confirms the presence of elemental cerium (Mo), oxygen (O) and carbon (C) in the sample.

3.4. UV-DRS spectrum

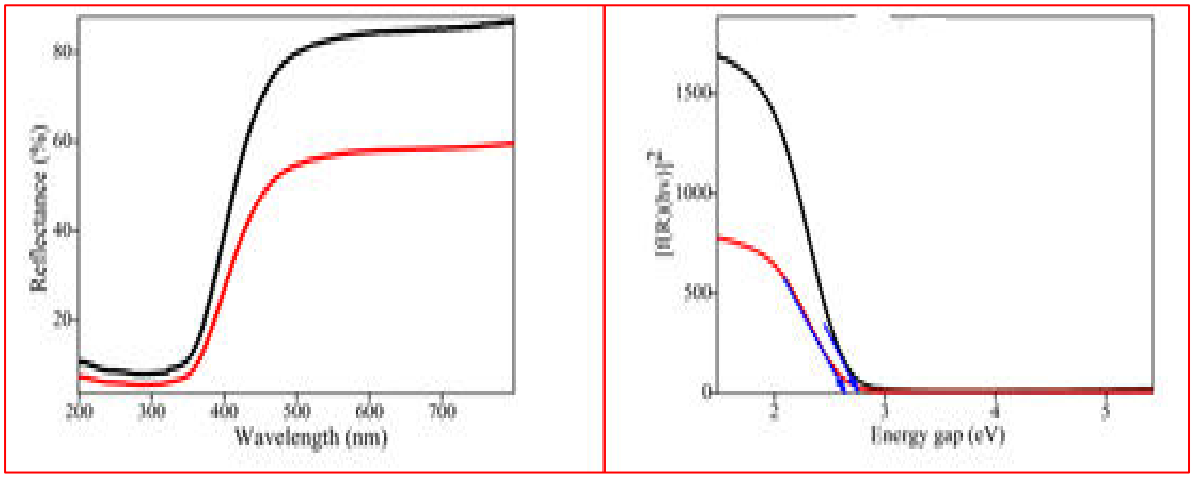

Fig.6. (a) UV DRS spectra (b) bandgap energy spectra of MoO_2 and MoO_2/rGO NCs.

Fig. 6a shows an absorption band in the 200-800 nm range for the nanocomposite. Reflectance data was used to calculate the bandgap energy (E_g), which is the energy differential between the valence band (VB) and conduction band (CB). The bandgap energy was determined to be 2.75 & 2.62 eV using Tauc's equation, as illustrated in Fig. 6b [43,44].

$$(\alpha h\upsilon)\ \gamma = A(h\nu - Eg)\text{---------}(8)$$

Here, α represents the absorption coefficient, h denotes Planck's constant, υ corresponds to the photon's frequency, A is a proportionality constant, and Eg signifies the bandgap energy, γ is nature of electronic transition which was considered as 2 for direct allowed transition. Also, by using Kubelka-Munk expression

$$(F(R\infty)h\nu)\ \gamma = A(h\nu\text{-}Eg)\text{----------}(9)$$

3.5. Electrochemical activity:

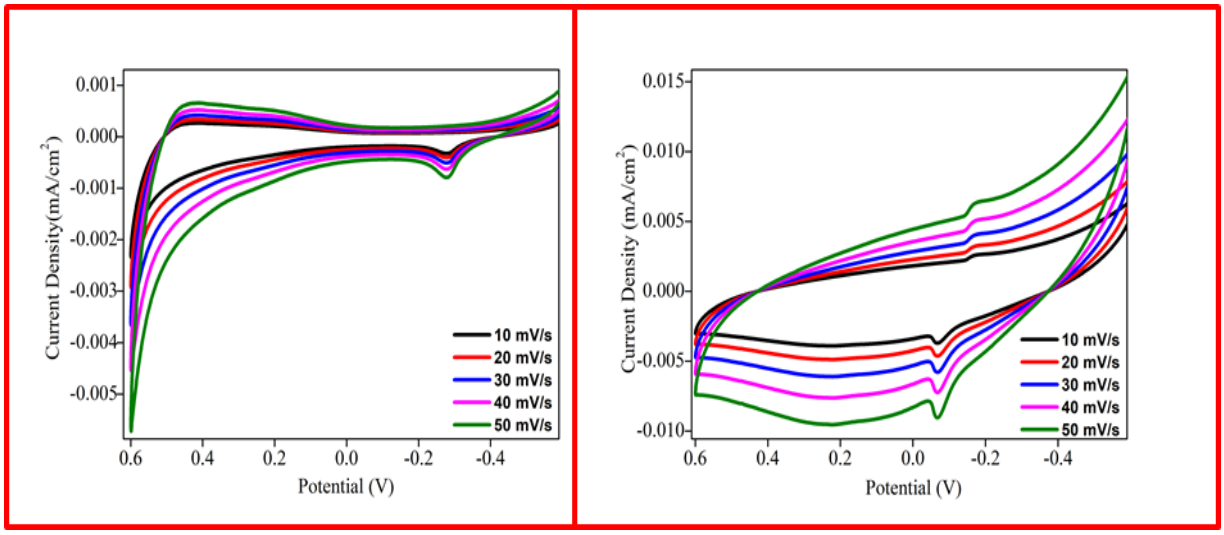

Fig.7. Cyclic voltammogram of (a) MoO_2 and (b) MoO_2/rGO NCs electrodes recorded at scan rates from 10, 20, 30, 40, 50 mV/s in 1M KOH electrolyte

The MoO_2 and MoO_2/rGO NCs were used as a modified working electrode for CV studies. The electrolyte used by the electrodes is 1 M KOH, and the scan rate ranges from 10 to 50 mV/s. In Fig.7 (a&b) the CV plots within the potential window of -0.5 to 0.6 V. MoO_2 and MoO_2/rGO NCs have smaller oxidation peaks at -0.2V and 0.1V, respectively. Excellent electrode stability is shown by the significant variation in the positions of the electrode's anodic peaks as the cycles go on [47, 48]. The cyclic voltammetry (CV) profiles of MoO_2 and MoO_2/rGO NCs exhibit well-defined redox peaks, indicating pseudocapacitive behaviour. The redox peaks observed can be attributed to the reversible transitions between Ce^{3+} and Ce^{4+} oxidation states. The anodic and cathodic peak positions remain nearly symmetric and stable over multiple scan rates, signifying good electrochemical reversibility and efficient charge transfer kinetics. This behavior underscores the suitability of the MoO_2/rGO NCs electrode for both supercapacitor and sensor applications.

4. Conclusions

MoO_2 and MoO_2/rGO NCs were successfully synthesized via hydrothermal method and structurally confirmed using XRD, HR-TEM, SEM, and DRS analyses. XRD revealed a face-centered cubic (Fm-3m) structure with high crystallinity. HR-TEM analysis showed a fringe width of 0.648 nm for the (040) plane, closely matching the theoretical value of 0.65 nm. SEM images displayed irregular, flower-like morphologies, and the optical bandgap were determined to be 2.75 eV (CeO_2) and 2.62 eV (MoO_2/rGO NCs), indicating enhanced charge transport in the composite. Electrochemical evaluation demonstrated excellent capacitive behavior, with MoO_2/rGO NCs achieving a specific capacitance of 245.1 Fg^{-1} at 1 Ag^{-1} in a three-electrode system, compared to 159.1 Fg^{-1} for pure MoO_2. The MoO_2/rGO NCs electrode exhibited superior cycling stability, retaining 95% capacitance after 2000 cycles.

References:

[1]. Montini, Tiziano, Michele Melchionna, Matteo Monai, and Paolo Fornasiero. "Fundamentals and catalytic applications of MoO_2-based materials." Chemical reviews 116, no. 10 (2016): 5987-6041.

[2]. Zhang, Yang, Shuna Zhao, Jing Feng, Shuyan Song, Weidong Shi, Dan Wang, and Hongjie Zhang. "Unraveling the physical chemistry and materials science of MoO_2-based nanostructures." Chem 7, no. 8 (2021): 2022-2059.

[3]. Ahn, Seon-Yong, Won-Jun Jang, Jae-Oh Shim, Byong-Hun Jeon, and Hyun-Seog Roh. "MoO_2-based oxygen storage capacity materials in environmental and energy catalysis for carbon neutrality: extended application and key catalytic properties." Catalysis Reviews 66, no. 4 (2024): 1316-1399.

[4]. Wang, Xianwei, Jingyi Wang, Yafei Sun, Kanghui Li, Tongxin Shang, and Ying Wan. "Recent advances and perspectives of MoO_2-based catalysts: Electronic properties and applications for energy storage and conversion." Frontiers in Chemistry 10 (2022): 1089708.

[5]. Lord, Megan S., Jean Francois Berret, Sanjay Singh, Ajayan Vinu, and Ajay S. Karakoti. "Redox active cerium oxide nanoparticles: current status and burning issues." Small 17, no. 51 (2021): 2102342.

[6]. Li, Zhi, Dongsheng Jia, Wei Zhang, Ying Li, Mitang Wang, and Dongliang Zhang. "Enhanced photocatalytic performance by regulating the Ce^{3+}/Ce^{4+} ratio in cerium dioxide." Frontiers of Chemical Science and Engineering 18, no. 3 (2024): 31.

[7]. Kowsuki, K., R. Nirmala, Yong-Ho Ra, and R. Navamathavan. "Recent advances in molybdinum oxide-based nanocomposites in synthesis, characterization, and energy storage applications: A comprehensive review." Results in Chemistry 5 (2023): 100877.

[8]. Mishra, Upendra Kumar, Vishal Singh Chandel, and Om Prakash Singh. "A review on cerium oxide–based catalysts for the removal of contaminants." Emergent Materials (2022): 1-34.

[9]. Arulkumar, Elumalai, and Sethuramachandran Thanikaikarasan. "Synthesis of CuO@ NiO/rGO nanocomposite with enhanced electrochemical and photocatalytic properties in energy and environmental applications." Journal of Alloys and Compounds 998 (2024): 175008.

[10]. Arulkumar, E., S. Thanikaikarasan, and E. V. Siddhardhan. "Synthesis and characterization of CuO@ NiO/g-C_3N_4 nanocomposite for photocatalytic and electrochemical application." Results in Chemistry 7 (2024): 101439.

[11]. Vinothini, Arunachalam, et al. "Biosynthesis of Cd and Ru doped MoO_2 nanoparticles with enhanced biomedical applications." Results in Chemistry 7 (2024): 101243.